High-voltage dilute ether electrolytes enabled by regulating interfacial structure

Huwei Wang[1], Jinkai Zhang[2], Haodong Zhang[1], Wei Li[1], Ming Chen[2], Qing Guo[3,4], Kah Chun Lau[3], Liang Zeng[2], Guang Feng[2,*], Dengyun Zhai[1,*], Feiyu Kang[1,*]

[1]Shenzhen Geim Graphene Center, Institute of Materials Research, Tsinghua Shenzhen International Graduate School, Tsinghua University, Shenzhen 518055, China.

[2]State Key Laboratory of Coal Combustion, School of Energy and Power Engineering, Huazhong University of Science and Technology (HUST), Wuhan, China.

[3]Department of Physics and Astronomy, California State University Northridge, CA, USA.

[4]Department of Physics, Michigan Technological University, MI, USA.

Correspondence: gfeng@hust.edu.cn (G.F.); zhaidy0404@sz.tsinghua.edu.cn (D.Z.); fykang@tsinghua.edu.cn (F.K.)

SUMMARY

Poor oxidation stability of ether solvents at the cathode restricts the use of dilute ether electrolytes with conventional concentrations around 1 M in high-voltage lithium metal batteries. Here we develop an anion-adsorption approach to altering the ether solvent environment within the electrical double layer (EDL) at the cathode, by adding a small amount of nitrate, so that the oxidation tolerance of nitrate-containing dilute ether electrolytes is enhanced up to 4.4 V (versus Li/Li$^+$), leading to complete compatibility with high-voltage cathodes and exhibiting superior cycling stability. Constant-potential molecular dynamics simulations reveal that ether molecules are mostly excluded from the cathode because of nitrate occupation in the inner layer of the EDL, thus suppressing ether oxidative decomposition. This work highlights that regulating the interfacial structure by adding surface adsorbates, rather than passivating cathode-electrolyte interphase or changing ion solvation, can help to enhance the oxidation stability of ether solvents. It also provides design criteria for adsorption-type additives to achieve high-voltage dilute ether electrolytes.

INTRODUCTION

Electrolytes are of great importance to various electrochemical energy storage systems, particularly high-energy-density lithium (Li) metal batteries (LMBs).[1,2] Among different electrolytes for LMBs (including solid-state or polymer electrolytes,[3,4] ionic liquids[5], and so on), conventional organic electrolytes are still the most widely used electrolytes for LMBs.[6-8] A promising electrolyte that is stable against reactive Li metal anode and high-voltage cathodes at the same time is highly desirable.[6,9] However, metallic Li is difficult to be compatible with commonly used organic carbonate solvents due to their low redox potential (-3.04 V versus the standard hydrogen electrode),[9-11] since solid-electrolyte interphase forms on the Li anode as a result of uncontrollable electrochemical reduction of carbonate electrolytes, which is chemically unstable and mechanically fragile.[6,8] To have better reductive stability with Li metal, ether solvents are undoubtedly more attractive for LMBs compared to carbonates.[12-14] However, conventional dilute ether electrolytes,[15,16] which have salt concentrations of around 1 M (M, moles per liter of solution), have long been excluded from being used with high-voltage cathodes, such as $LiCoO_2$ and $LiNi_xMn_yCo_{1-x-y}O_2$ (NMC), due to their low oxidation stability (less than 4 V vs. Li/Li^+).[8] Consequently, dilute ether electrolytes have usually been utilized in LMBs with cathodes below 4 V (for example, $LiFePO_4$ and sulfur).[17,18] Therefore, research on the design of dilute ether electrolytes with extraordinary oxidation stability has drawn much attention and become one of the frontiers in the battery community.[19]

The early entry of ether electrolytes for high-voltage LMBs adopted the high-concentration formulations (*e.g.*, triglyme and tetraglyme solvents with equimolar Li salt).[20] Although the oxidation stability can be improved to ~5 V on the platinum electrode, only limited cycling stability (200 cycles) was achieved on the $LiCoO_2$ cathode with a cutoff voltage of 4.2 V. Until now, the high-concentration ether electrolytes[14,21,22] and localized high-concentration ether electrolytes[23,24] effectively developed for 4.3/4.4 V NMC cathodes have all followed the same design concept, namely, high salt/solvent molar ratio.[16] Meanwhile, elimination of unbound (free) solvents of electrolyte[16,22] and formation of stable cathode-electrolyte interphase (CEI)[13,14,21,23] have become generally accepted views on the improved oxidation stability. In particular, the high-concentration ether electrolytes usually suffer from

57 the economic effectiveness, high viscosity and slow dynamics.[15,16] Even for the localized high-

58 concentration electrolyte formulation evaluated for practical applications,[23,24] the usage of

59 hydrofluoroether diluents still results in possible environmental hazards.[25] Hence, compared with these

60 salt-concentrated solutions, dilute ether electrolytes are thus long required to have high-voltage

61 tolerance; however, limited by their intrinsic poor oxidation stability,[8] such achievements are rarely

62 reported.[19] Recently, a molecular design strategy was proposed by introducing fluorinated segment

63 into the ether backbone to improve the oxidation stability of ether.[26,27] These delicately designed ether

64 electrolytes share the common feature of high-voltage tolerance with the hydrofluoroethers. As a

65 consequence, at 1 M salt concentration, these amended ethers have been successfully used with

66 NMC811 cathodes with cutoff voltages up to 4.4/4.6/4.8 V. This molecular design concept is a

67 remarkable breakthrough in ether electrolyte engineering; however, the changes of ether are often not

68 easily handled due to their delicate synthesis technique. Therefore, a simple handling design for

69 achieving high-voltage electrolytes in 1 M salt concentration with ether solvent unchanged is still

70 highly desired.

71   To achieve this goal, we develop a strategy based on anion adsorption to alter the ether solvent

72 environment within the electrical double layer (EDL) at the cathode. This strategy enables the

73 enhancement of oxidation stability in 1 M imide salt-based 1,2-dimethoxyethane (DME) electrolytes

74 up to 4.3 V, only by adding a small amount of nitrate. The LMBs coupled with high-voltage $LiCoO_2$

75 and NMC532 cathodes in these dilute ether electrolytes exhibit superior cycling stability. Although

76 many promising properties of nitrate for Li metal anodes have been reported,[28-31] very limited progress

77 has been made on nitrate interfacial behavior near the cathode surface. Here, experimental

78 measurements and molecular simulations were combined to elucidate that by regulating the interfacial

79 structure at the cathode, added NO_3^- could suppress the ether oxidative decomposition, although the

80 additive has little influence on the bulk electrolyte. As a proof of concept, beyond NO_3^-, we

81 experimentally demonstrated that a series of anions, including ClO_4^-, ClO_3^-, $H_2PO_4^-$ and HPO_4^{2-}, have

82 similar effects on improving the oxidation stability of ethers. This electrolyte design concept would

83 provide insights into the high-voltage application of low concentration electrolytes in LMBs.

84 Furthermore, this understanding of the electrified interfaces at the molecular level may be applicable

85   to the community of electrochemistry beyond the battery, such as the electrocatalysis[32] and

86   electrosynthesis[33].

87   **RESULTS AND DISCUSSION**

88   **Enhanced high-voltage tolerance of ether electrolyte by adding tiny nitrate**

89   High-voltage tolerance was first evaluated in the cyclic voltammetry (CV) and linear sweep

90   voltammetry (LSV) tests on Li||LiCoO$_2$ and Li||Al cells, respectively (Figure 1A and Figure S1). When

91   using the LiCoO$_2$ electrode as the working electrode, unlike the low oxidation onset voltage of ~3.9 V

92   for pristine ether electrolytes of 1 M lithium bis(trifluoromethanesulfonyl)imide (LiTFSI) in DME, the

93   ether electrolyte with 50 mM NO$_3^-$ showed greatly improved oxidation stability by giving a cutoff

94   voltage at 4.4 V (Figure 1A). To assess the feasibility of adding the nitrate to enable the dilute ether

95   electrolyte under high voltages, LMBs, with a LiCoO$_2$ cathode and 1 M LiTFSI in DME, were cycled

96   at a high charge cutoff voltage of 4.3 V. A low cathode areal loading of 0.3 mAh cm^{-2} and excess Li

97   were used to ensure only a small amount of Li metal was cycled, the impact of electrolyte stability on

98   the Li anode is deliberately minimized.[34] As shown in Figure 1B, in only the 7th cycle, the cell with

99   the nitrate-free dilute ether electrolyte failed to reach the cutoff voltage (<4.2 V), demonstrating that

100   the conventional dilute ether electrolyte has extremely poor high-voltage compatibility. In stark

101   contrast, the NO$_3^-$-containing ether electrolyte (*i.e.*, 1 M LiTFSI/DME with 50 mM LiNO$_3$) could

102   achieve 93% capacity retention with a limited polarization increase (Figure S2) after 1000 cycles. In

103   addition to LiCoO$_2$ cathodes, remarkable high-voltage stability (1000 cycles with 89% capacity

104   retention) was also found in the long-term cycling of NMC532 cathodes (Figure 1D). Furthermore,

105   microscopy images proved that Al foil cycled in the NO$_3^-$-containing dilute ether electrolyte remains

106   intact, whereas pitting corrosion occurred in the pristine ether electrolyte (Figure S3). These results

107   prove the robustness of NO$_3^-$-containing dilute ether electrolyte under high voltages. Note that because

108   of the poor oxidation stability of the pristine ether electrolyte at high voltages (Figure 1B and Figure

109   S4), it was not studied further in electrochemical cells.

110   **Little change of CEI stability and ion solvation**

111 Since ether solvent typically decomposes as voltage exceeds 4.0 V (refs.[8,14,19,21]), it is intriguing to

112 unveil how such a small amount of NO_3^- could boost the oxidation stability of the conventional dilute

113 ether electrolyte at the cathode. Considering that the current common views of electrolyte design,

114 especially with regard to the well-understood salt-concentrated electrolytes, mostly focus on

115 passivating CEI[14,21,23] or changing electrolyte ion solvation[16], similar mechanisms are worthy of being

116 checked here. The first concern is whether a stable protective CEI film is formed in the NO_3^--

117 containing ether electrolyte. We probed the surface structure of the cycled $LiCoO_2$ cathode in NO_3^--

118 containing ether electrolytes using the transmission electron microscope (TEM). Compared to the

119 surface morphology of the bare $LiCoO_2$ (Figure 2A), a clear and intact surface edge can be observed

120 in the representative region of the cycled $LiCoO_2$ (Figure 2B) — a selected region based on extensive

121 TEM characterizations; while in some local regions, a nonuniform amorphous layer (2–10 nm) and

122 gathered nanoscale crystalline grains (assigned to LiF) can be found (Figure S5). The poor

123 homogeneity cannot support the conclusion that an effective surface passivating layer forms in the

124 NO_3^--containing ether electrolyte.

125 Meanwhile, the surface chemistry of the cycled $LiCoO_2$ electrodes was probed via the X-ray

126 photoelectron spectroscopy (XPS) measurement. As seen from the fitted O 1s XPS spectra in Figure

127 S6A, compared with the bare $LiCoO_2$ electrode, lattice oxygen at 529.8 eV (shaded area) shows a

128 flatter peak in the cycled $LiCoO_2$ electrodes (50 cycles). The signals (C-O and C=O) from the CEI

129 components overwhelm the lattice oxygen peak, implying the electrolyte decomposition on the $LiCoO_2$

130 surface.[35,36] However, the inorganic signals, especially for the LiF species (56.0 eV in Li 1s and 684.8

131 eV in F 1s, Figures S6B and S6C), are not particularly noticeable. This surface can only be identified

132 as an organic-inorganic hybrid surface, which is distinct from the inorganic-dominated surface

133 observed in the salt-concentrated ether electrolytes for high-voltage LMBs.[21,23] To further confirm the

134 stability of this surface, the $LiCoO_2$ electrodes pre-polarized in the NO_3^--containing ether electrolyte

135 were carefully reassembled in the NO_3^--free ether electrolyte for sequential cycling (Figure S7).

136 Unfortunately, without the presence of nitrate, the cell with pre-polarized electrode fails to reach the

137 cut-off voltage within the first cycle (Figures S7B and S7D), which is consistent with the behavior

138 observed in Figure 1B. This failure confirms that the surface passivating formed in the NO_3^--containing

139 ether electrolyte is not stable enough.

140   Moreover, the chemical environment of DME molecules, a frequently mentioned issue in

141 electrolyte design,[16] is also examined by nuclear magnetic resonance (NMR) spectroscopy. At 1 M

142 LiTFSI electrolyte, the peak of O_{DME} shifts upfield with the increase of $LiNO_3$ concentration (Figure

143 2C). However, this upfield shift was weakly indistinguishable when only 50 mM $LiNO_3$ was added,

144 suggesting a weakly changed chemical environment of DME in the bulk electrolyte. Even when the

145 concentration of $LiNO_3$ increases to 200 mM, this upfield shift remains unnoticeable. Such

146 phenomenon is further confirmed by molecular dynamics (MD) simulations of bulk ether electrolytes,

147 where the number density of DME around Li^+ is slightly changed when adding 50 mM $LiNO_3$ and

148 almost unchanged with $LiNO_3$ concentration increasing from 50 mM to 200 mM (Figure 2D). The

149 detailed coordination states are represented in Figure 2E and 2F, and Figure S8C, where NO_3^- partly

150 replaces $TFSI^-$ anion but the coordination between Li^+ and DME is maintained. Until the $LiNO_3$

151 concentration reaches 500 mM, the replacement of DME by NO_3^- in the first solvation shell takes place

152 (Figure 2G). These results demonstrate a slight change of electrolyte ion solvation with additive, which

153 also fails to explain the great improvement of oxidation stability.

154   Overall, the presence of a small amount of NO_3^- has little influence on either stable CEI formation

155 or the ion solvation environment in bulk electrolytes, the enhanced oxidation stability of the $LiNO_3$-

156 containing dilute electrolyte cannot be explained with current knowledge developed in the salt-

157 concentrated electrolytes.

158 **Regulation of interfacial structure by added nitrate**

159 Considering that the electrolyte reactivity originates from the solvent contacting the cathode, a

160 thorough understanding of the aggregation state of different solvent molecules or ions at the electrified

161 interface becomes very crucial.[31,37,38] MD simulations with the implementation of the constant

162 potential method[39] for asymmetric electrode systems with Li metal anode and $LiCoO_2$ cathode,

163 depicted in Figure S9, were adopted to dissect the EDL structure of pristine and NO_3^--containing 1 M

164 LiTFSI in DME at the cathode. For the pristine ether electrolyte, under the positive polarization, a

165 distinct layer of DME molecules within ~0.5 nm could contact the cathode (Figure 3A), with the vector

166 between two O atoms of a DME molecule mainly parallel to the cathode surface (Figure S10); while

167 with adding a small amount of NO_3^-, the DME at the cathode is found to be drastically reduced, as

168 illustrated in Figure 3A. Meanwhile, a large accumulation of NO_3^- anions can be found at the cathode

169 surface, driven by the positive polarization (Figure 3B); interestingly, the number ratio of interfacial

170 NO_3^- to $TFSI^-$ is 0.83 (from the integration of number density in Figure S11), which is far above the

171 ratio in the bulk region (0.2), this remarkable increase of NO_3^- anions at interface implies the

172 preferential absorption of NO_3^- for $LiCoO_2$. More importantly, this finding indicates that the interfacial

173 features of NO_3^--containing ether electrolyte does not inherit chemical signatures from bulk solution,

174 which is qualitatively different from the high-/super-concentrated electrolytes[40-43]. This preferential

175 absorption of NO_3^- can be explained by the lower free energy of interfacial NO_3^- than $TFSI^-$ (Figure

176 S12), which may result from the geometric shape/size of anions and delocalized intrinsic charge of the

177 cathode (Figures S9A and S9B). However, the Li^+ ion peak becomes unexpectedly higher, which could

178 be understood by the attraction from accumulated NO_3^- anions and their strongest interaction with Li^+

179 (Figure S13). At higher electrode polarization (2.0 V), a similar response is detected for the presence

180 of anions, cations, and DME molecules (Figure S14).

181   The notable accumulation of NO_3^- anions and remarkable decrease of DME molecules at the

182 positively polarized $LiCoO_2$ indicate a competition between NO_3^- entering and DME leaving from the

183 inner layer of EDL. The accumulation of NO_3^- anions reduces the number of DME molecules, because

184 the occupation of NO_3^- ions with their associated Li^+ ions squeezes out DME on the cathode (Figures

185 3A and 3B, and Figure S11). These results provide a qualitative picture: at the cathode surface, the

186 added NO_3^- anions associated with more Li^+ ions occupy the space of the inner layer of EDL,

187 minimizing the solvent decomposition,[42,44] as schematized in Figure 3C and 3D.

188   To gain deeper insight into the role of added NO_3^-, we further introduced LiI into these ether

189 electrolytes with and without NO_3^- (Figure S15A). Adding LiI reduces the oxidation onset potential of

190 pristine ether electrolyte from 3.9 to 2.95 V. As NO_3^- and I^- anions coexist, the onset potential for I^-

191 anions oxidation shifts towards more positive potentials from 2.95 to 3.5 V, confirming competing

192 adsorption between NO_3^- and I^- anions. Nevertheless, the oxidation onset potential is always less than

8

193 3.9 V with the presence of I⁻, suggesting that the easily oxidized I⁻ anions are more likely to contact

194 the cathode surface and dominate interfacial oxidation. This result re-emphasizes the importance of

195 the adsorbate in the oxidation behavior of the electrolyte. Furthermore, by increasing the concentration

196 of NO_3^- in the electrolyte (at fixed main salt concentration of 1 M), the oxidation slowly takes off with

197 its onset potential shifting towards more positive values at higher NO_3^- content (Figure S15B),

198 providing further evidence for competitive adsorption. The detailed mechanisms are illustrated in

199 Figures S15C–15D. These observations are qualitatively consistent with the anion-adsorption

200 mechanism inferred from MD simulations. Additionally, the adsorbability of NO_3^- was verified by a

201 steady-state NO_3^- anion adsorption experiment without external electrode potential, where a lower

202 NO_3^- concentration near the gathered $LiCoO_2$ electrodes can be quantified than in the bulk solution

203 (Note S2 and Figure S16).

204 Altogether, our combined experimental and modeling observations unveil the crucial role of NO_3^-

205 -adsorbed interfacial structure on the ether reactivity and provide a picture at the molecular level of

206 the NO_3^-–anion adsorption behavior at the electrochemical interfaces: that is, the added nitrate would

207 little change the ion solvation in bulk electrolyte but could significantly regulate the EDL structure to

208 inhibit ether oxidative decomposition at the cathode. Meanwhile, it is worth noting that, unlike in the

209 case of super-concentrated aqueous electrolytes,[41-43] the interfacial chemical signatures in dilute

210 electrolytes do not inherit from the bulk solution.

211 **Cell performances of LMBs with NO_3^--containing ether electrolytes**

212 The highly important merit of high-voltage tolerance brought by adding NO_3^- in the dilute ether

213 electrolytes can be best signified when testing LMBs with high-loading cathodes. Figure 4 exhibits

214 extremely stable cycling performances of Li‖cathodes cells consisting of a medium-high cathode areal

215 loading of 1.3–1.4 mAh cm⁻² and NO_3^--containing dilute ether electrolytes. The Li‖$LiCoO_2$ cell in the

216 ether electrolyte with 200 mM $LiNO_3$ showed high capacity retention (95.5%) (Figure 4A) and a small

217 polarization (Figure S17A) after 300 cycles. Meanwhile, only a trace amount of electrolyte under this

218 condition has been decomposed (maximum mass fraction per cycle < 0.022 wt%, see Note S3 for

219 details). Notably, although this oxidative breakdown did not gradually weaken or halt (Figure S18), it

220 did not result in continuous undesired cathode capacity fading. Furthermore, this ether electrolyte

221 successfully enabled stable cycling of Li||NMC532 under 4.3 V for 300 cycles (Figures 4B). To the

222 best of our knowledge, this is the first demonstration that long-term stability of LMB with DME-based

223 ether electrolyte at such low concentration can be obtained under a cutoff voltage of 4.3 V. Admittedly,

224 the reported test conditions still fall short of the stringent requirements of practical LMBs (lean

225 electrolyte, thin Li, and > 3 mAh cm^{-2} cathode loading).[6,24]. Nevertheless, the effectiveness of our

226 proposed anion-adsorption strategy for increasing the high-voltage tolerance of dilute ether electrolytes

227 is clear from the electrochemical measurements. Further improvements can be gained when NO_3^--

228 containing ether electrolytes are used in combination with other strategies for Li metal stabilization,

229 such as nanostructuring the electrode[11] and coordinating different salts[17].

Generality of strategy

231 To assess the generality of this nitrate additive strategy, different types of main salts and ether

232 electrolyte systems were chosen. The lithium bis(fluorosulfonyl)imide (LiFSI)-based dilute

233 electrolytes with NO_3^- showed good compatibility with $LiCoO_2$ and NMC532 cathodes under a cutoff

234 voltage of 4.3 V, realizing high capacity retentions of 94.2% and 90.4%, respectively, for over 600

235 cycles (Figure S19). More importantly, high-voltage tolerance of 4.3 V was also confirmed in the

236 sodium (Na)-ion electrolyte system (Figure S20). 1000-cycle Na-ion battery with Na Prussian blue

237 (NaPB) was achieved in 1 M $NaPF_6$ DME with 50 mM $NaNO_3$. These results illustrate the feasibility

238 of our strategy by adding tiny NO_3^- to increase the high-voltage tolerance of dilute ether electrolytes.

239 Beyond the nitrate, are there more additives? Could rational criteria be proposed for identifying

240 appropriate additives? To answer these questions, we carried out a number of electrochemical

241 experiments to employ a series of inorganic salts as additives to alter the ether solvent environment in

242 EDLs (see Table S1 for detailed classification of salts). Considering that involvement of I^- hampers

243 the packing of the NO_3^- adsorption layer (Figure S15A), the oxidation tolerance of the anion itself is

244 taken into account first; for instance, oxidation of N (III) in NO_2^- rather than N (VI) in NO_3^- is favored

245 thermodynamically. As shown in Figures S22A and S22C, the LSV for $NaNO_2$-containing ether

246 electrolyte exhibited a weak current response early at ~3.9 V, with two new oxidation peaks appearing

10

247 at high potentials. The detailed investigation suggests that the irreversible oxidation of $NaNO_2$ salt

248 accounts for the appearance of these peaks (Figures S22D and S22E). Even though the overall onset

249 of oxidation of this $NaNO_2$-containing ether electrolyte becomes ~0.2 V higher than in the presence of

250 $LiNO_3$ (Figure S22A), further attempts to test the cycling stability of this electrolyte in Li||LiCoO_2

251 proved fruitless (Figure S22B). Meanwhile, better oxidation stability of $LiClO_4$ than $NaClO_3$ was

252 experimentally confirmed by a higher onset potential of oxidation in the $LiClO_4$-containing ether

253 electrolytes (Figure S23). As for the Na_2SO_4 with S (VI) and $AlPO_4$ with P (V) (two types of

254 soluble/slightly soluble salts with high valence state, Table S1), they failed to enhance the oxidation

255 stability of the ether electrolytes. But interestingly, KH_2PO_4 and K_2HPO_4 with P (V) enabled improved

256 oxidation tolerance of the dilute ether electrolytes (Figure S24). Finally, except for the undissolved

257 salts in ethers, the oxidation stability was experimentally found to increase with the presence of five

258 salts, including $LiNO_3$, $LiClO_4$, $NaClO_3$, KH_2PO_4 and K_2HPO_4, where the maximum enhancement

259 was obtained when $LiClO_4$ salt was used (Table S1).

260 To delve into the difference of these resultful additives, a plot of the onset shift as a function of

261 corresponding anion radius is shown in Figure 5 (see Figure S21 for the confirmation of onset

262 potential). A nearly linear decrease of the onset shift with increased anion radius highlights the

263 importance of ion size in adsorption. As for the abnormal trend of $LiClO_4$, specific adsorption

264 (normally occurs in the IHP[45]) rather than electro-adsorption may account for its interfacial as well as

265 electrochemical behavior. Combined with results of competitive adsorption in the presence of LiI, we

266 can therefore reach four requirements for additive selection/design that should be simultaneously met:

267 (1) certain solubility in ether electrolytes, (2) high oxidation stability of anions, (3) strong specific

268 adsorption/electro-adsorption ability with (4) small geometric size for lowering the steric barrier.

269 **Conclusion**

270 We have developed dilute ether electrolytes by adding a small amount of NO_3^- anions for long-term

271 cycling of LMBs under voltages as high as 4.3 V, which break the long-standing voltage limitation for

272 dilute ether electrolytes. Our combined experimental and modeling results have uncovered that

273 accumulation of added NO_3^- in the inner layer of EDL at the cathode is important to squeeze out DME

274   molecules at the cathode and thus suppresses the ether reactivity.

275   This study reveals new surface chemistry in the dilute ether electrolyte — surface adsorbates matter

276   to alter the solvent environment at a polarized cathode. This picture is qualitatively different from the

277   high-/super-concentrated electrolytes, where their interfacial features inherit chemical signatures from

278   bulk solution, namely, anions instead of solvent molecules dominated;[40-43] while the interfacial

279   chemistry of dilute electrolytes with additives in this study is primarily dominated by the oxidation of

280   solvent molecules.[15] Therefore, in the presence of additives, the purely anion-adsorption mechanism

281   should start to become primary, highlighting the crucial role of anion-regulated interfacial feature

282   rather than the nature of bulk solution on the solvent stability in the electrochemical device using dilute

283   electrolytes.

284   Our findings point to the value of regulating the surface adsorbates at the cathode to control the

285   interfacial nanostructure and consequently the solvent reactivity. This paves a new way for designing

286   "adsorption-type" additives for high-voltage dilute ethers, since there are a huge number of possible

287   surface adsorbates that can be employed to fine-tune the interfacial nanostructure and hence control

288   interfacial electrochemical reactivity. This acquired knowledge extends the understanding of dilute

289   electrolytes and their design, which could be used for a wide variety of electrochemical devices for

290   improved safety (for instance, dendrite suppression in Zn batteries[46]), controllable reactivity (for

291   instance, enhanced oxygen reduction[32] or weakened water reduction[47]), or increased selectivity (for

292   instance, CO_2 reduction[48]).

EXPERIMENTAL PROCEDURES

Electrolyte and electrode preparation. LiFSI was purchased from Fluolyte and Smooth Way; LiTFSI, LiPF$_6$, NaPF$_6$, MgSO$_4$, Na$_2$SO$_4$, NaHSO$_3$, NaClO$_3$, KH$_2$PO$_4$, NaNO$_2$, NaNO$_3$, DME, and diethylene glycol dimethyl ether (G2) were purchased from Sigma-Aldrich; LiNO$_3$ and AlPO$_4$ were purchased from Alfa Aesar; LiI and LiClO$_4$ were purchased from Aladdin; LiOTf and LiBF$_4$ were purchased from TCI; LiPO$_3$ and Li$_3$PO$_4$ were purchased from Energy Chemical; K$_2$HPO$_4$ was purchased from Acros. DME and G2 solvents were dried over 4 Å molecular sieves (Sigma-Aldrich) prior to preparing electrolytes. The electrolytes were prepared by dissolving the selected (mixture) salts in the DME/G2 solvent in an argon gas-filled glove box (MBraun) with oxygen and moisture contents below 0.1 ppm.

LiCoO$_2$ and LiNi$_{0.5}$Mn$_{0.3}$Co$_{0.2}$O$_2$ (NMC532) cathode materials were purchased from Canrd and used as received. The laminate of low/medium-high loading LiCoO$_2$ electrodes (~1.9/~9.3 mg active material cm^{-2}) and NMC532 electrodes (~1.9/~9.8 mg active material cm^{-2}) were prepared by casting a slurry mixture containing 90 wt% active material, 5 wt% carbon black (Super P, Canrd) and 5 wt% polyvinylidene difluoride (PVdF, Canrd) in N-methylpyrrolidone onto an aluminum (Al) foil. After drying at 110 $^{\circ}$C under vacuum for 12 h, the electrodes were cut into discs with a diameter of 12 mm. Thick Li foil (450 μm thickness, 1.56 cm diameter) was purchased from MTI. NaPB was synthesized following a previous report[49]. The areal mass loading of NaPB in the electrode was ~1 mg cm^{-2}.

Electrochemical measurements. Li‖LiCoO$_2$ and Li‖NMC532 cells were assembled in the standard CR2032 coin-type cells, with thick Li foil (450 μm) as the anode, one-piece separator (Celgard2400) separator and the prepared electrolyte (70 μL in each cell). The Li‖LiCoO$_2$ and Li‖NMC532 cells were tested in constant-current mode on battery testers (Wuhan LAND) within the voltage range of 3.0–4.3 V and 2.8–4.3 V, respectively. Only for the Li‖NMC532 cells with medium-high loading electrodes, a constant-current-constant-voltage mode was used; cells were charged to 4.3 V and then held at 4.3 V until the charge current decayed to C/10, where 1C is equal to 180 mA g^{-1}. LSV studies of the electrolytes were conducted on a Biologic VMP3 system. Electrochemical impedance spectroscopy (EIS) was conducted in a three-electrode cell (ECC-ref cell (EL-CELL)) configuration using a Solartron 1470E workstation.

Characterizations. Morphological characterization was performed using optical microscopy (Carl Zeiss Microscopy, Germany), SEM (HITACHI SU8010, Japan), and high-resolution TEM (FEI Tecnai G2 F30, USA). ^{17}O NMR data were obtained on a Bruker Avance 400 MHz NMR spectrometer. 400 μL electrolyte was put into 5 mm NMR tube with 150 μL deuterium oxide (D$_2$O) as an external reference in a coaxal insert tube (NORELL). XPS analysis was obtained on a PHI 5000 VersaProbe II spectrometer using monochromatic Al Kα X-ray source. Before conducting SEM, TEM, and XPS studies of cycled electrodes, cells were disassembled in the glovebox, and the obtained electrodes were rinsed with DME to remove residue salts. The cross-sections of Li anodes were obtained by cutting the Li foils with a razor blade. Air-free transfer vessels were used to avoid any contamination from the air. Ultraviolet-visible spectrophotometer (UV-vis, Agilent Cary5000, USA) was used to quantify the concentration of NO$_3^-$ based on its absorbance at 297 nm.

Molecular dynamics simulation. Molecular dynamics simulations were performed to investigate the molecular structure of bulk and interfacial region on the cathode, using MD package GROMACS[50]. The schematic of system are shown in Figures S8A and S8B. For the electrode-electrolyte system, the constant potential method was implemented[39] in GROMACS and further developed for asymmetric electrode systems. The force field for

the electrolyte is developed by Dzubiella *et al.*[51], which can satisfactorily reproduce density, dielectric constant, viscosity, and diffusion coefficient of LiTFSI/LiNO$_3$/DME/DOL mixtures measured by experiments. The parameters for the van-der-Waals potential of LiCoO$_2$ cathode are taken from the UFF force field[52], and those for Li metal anode are taken from ref[53]. While the structure and intrinsic charge of Li metal anode and LiCoO$_2$ cathode are optimized using the density functional theory (DFT) with results shown in Figure S9. The details for simulations are presented in Note S1.

ACKNOWLEDGEMENTS

AUTHOR CONTRIBUTIONS

H.W. conceived the idea and designed the experiments; G.F. designed the modeling. D.Z. and F.K. directed the project. H.W. performed SEM experiments, electrochemical measurements, and coin-cell tests. H.Z. and W.L. performed the XPS measurements, collected the ^{17}O-NMR spectra and ultraviolet-visible spectra. J.Z. and L.Z. performed MD simulations. M.C., Q.G., and K.C.L. performed DFT simulations. H.W., J.Z., and G.F. wrote the manuscript. All authors contributed to discussing data, editing, and revising the paper.

DECLARATION OF INTERESTS

The authors declare no competing interests.

REFERENCES

1. Armand, M., and Tarascon, J.M. (2008). Building better batteries. Nature *451*, 652-657.
2. Dunn, B., Kamath, H., and Tarascon, J.-M. (2011). Electrical energy storage for the grid: a battery of choices. Science *334*, 928-935.
3. Croce, F., Appetecchi, G.B., Persi, L., and Scrosati, B. (1998). Nanocomposite polymer electrolytes for lithium batteries. Nature *394*, 456-458.
4. Dixit, M.B., Zaman, W., Hortance, N., Vujic, S., Harkey, B., Shen, F., Tsai, W.-Y., De Andrade, V., Chen, X.C., Balke, N., and Hatzell, K.B. (2020). Nanoscale mapping of extrinsic interfaces in hybrid solid electrolytes. Joule *4*, 207-221.
5. Armand, M., Endres, F., MacFarlane, D.R., Ohno, H., and Scrosati, B. (2009). Ionic-liquid materials for the electrochemical challenges of the future. Nat. Mater. *8*, 621-629.
6. Liu, J., Bao, Z., Cui, Y., Dufek, E.J., Goodenough, J.B., Khalifah, P., Li, Q., Liaw, B.Y., Liu, P., Manthiram, A., et al. (2019). Pathways for practical high-energy long-cycling lithium metal batteries. Nat. Energy *4*, 180-186.
7. Zhao, Q., Stalin, S., and Archer, L.A. (2021). Stabilizing metal battery anodes through the design of solid electrolyte interphases. Joule *5*, 1119-1142.
8. Xu, K. (2014). Electrolytes and interphases in Li-ion batteries and beyond. Chem. Rev. *114*, 11503-11618.
9. Lin, D., Liu, Y., and Cui, Y. (2017). Reviving the lithium metal anode for high-energy batteries. Nat. Nanotechnol. *12*, 194-206.
10. Heiskanen, S.K., Kim, J., and Lucht, B.L. (2019). Generation and evolution of the solid electrolyte interphase of lithium-ion batteries. Joule *3*, 2322-2333.
11. Lin, D., Liu, Y., Liang, Z., Lee, H.-W., Sun, J., Wang, H., Yan, K., Xie, J., and Cui, Y. (2016). Layered reduced graphene oxide with nanoscale interlayer gaps as a stable host for lithium metal anodes. Nat. Nanotechnol. *11*, 626-632.
12. Qian, J., Henderson, W.A., Xu, W., Bhattacharya, P., Engelhard, M., Borodin, O., and Zhang, J.-G. (2015). High rate and stable cycling of lithium metal anode. Nat. Commun. *6*, 6362.
13. Cao, X., Ren, X., Zou, L., Engelhard, M.H., Huang, W., Wang, H., Matthews, B.E., Lee, H., Niu, C., Arey, B.W., et al. (2019). Monolithic solid-electrolyte interphases formed in fluorinated orthoformate-based electrolytes minimize Li depletion and pulverization. Nat. Energy *4*, 796-805.
14. Jiao, S., Ren, X., Cao, R., Engelhard, M.H., Liu, Y., Hu, D., Mei, D., Zheng, J., Zhao, W., Li, Q., et al. (2018). Stable cycling of high-voltage lithium metal batteries in ether electrolytes. Nat. Energy *3*, 739-746.
15. Borodin, O., Self, J., Persson, K.A., Wang, C., and Xu, K. (2020). Uncharted waters: super-concentrated electrolytes. Joule *4*, 69-100.
16. Yamada, Y., Wang, J., Ko, S., Watanabe, E., and Yamada, A. (2019). Advances and issues in developing salt-concentrated battery electrolytes. Nat. Energy *4*, 269-280.
17. Qiu, F., Li, X., Deng, H., Wang, D., Mu, X., He, P., and Zhou, H. (2019). A concentrated ternary-salts electrolyte for high reversible Li metal battery with slight excess Li. Adv. Energy Mater. *9*, 1803372.
18. Zhang, S.S. (2012). Role of $LiNO_3$ in rechargeable lithium/sulfur battery. Electrochim. Acta *70*, 344-348.
19. Fan, X., and Wang, C. (2021). High-voltage liquid electrolytes for Li batteries: progress and perspectives. Chem. Soc. Rev. *50*, 10486-10566.
20. Yoshida, K., Nakamura, M., Kazue, Y., Tachikawa, N., Tsuzuki, S., Seki, S., Dokko, K., and Watanabe, M. (2011). Oxidative-stability enhancement and charge transport mechanism in glyme-lithium salt equimolar

15

397   complexes. J. Am. Chem. Soc. *133*, 13121-13129.

398 21. Ren, X., Zou, L., Jiao, S., Mei, D., Engelhard, M.H., Li, Q., Lee, H., Niu, C., Adams, B.D., Wang, C., et

399   al. (2019). High-concentration ether electrolytes for stable high-voltage lithium metal batteries. ACS

400   Energy Lett. *4*, 896-902.

401 22. Alvarado, J., Schroeder, M.A., Pollard, T.P., Wang, X., Lee, J.Z., Zhang, M., Wynn, T., Ding, M., Borodin,

402   O., Meng, Y.S., and Xu, K. (2019). Bisalt ether electrolytes: a pathway towards lithium metal batteries with

403   Ni-rich cathodes. Energy Environ. Sci. *12*, 780-794.

404 23. Ren, X., Zou, L., Cao, X., Engelhard, M.H., Liu, W., Burton, S.D., Lee, H., Niu, C., Matthews, B.E., Zhu,

405   Z., et al. (2019). Enabling high-voltage lithium-metal batteries under practical conditions. Joule *3*, 1662-

406   1676.

407 24. Niu, C., Liu, D., Lochala, J.A., Anderson, C.S., Cao, X., Gross, M.E., Xu, W., Zhang, J.-G., Whittingham,

408   M.S., Xiao, J., and Liu, J. (2021). Balancing interfacial reactions to achieve long cycle life in high-energy

409   lithium metal batteries. Nat. Energy *6*, 723-732.

410 25. Tsai, W.T. (2005). Environmental risk assessment of hydrofluoroethers (HFEs). J. Hazard. Mater. *119*, 69-

411   78.

412 26. Amanchukwu, C.V., Yu, Z., Kong, X., Qin, J., Cui, Y., and Bao, Z. (2020). A new class of ionically

413   conducting fluorinated ether electrolytes with high electrochemical stability. J. Am. Chem. Soc. *142*, 7393-

414   7403.

415 27. Yu, Z., Wang, H., Kong, X., Huang, W., Tsao, Y., Mackanic, D.G., Wang, K., Wang, X., Huang, W.,

416   Choudhury, S., et al. (2020). Molecular design for electrolyte solvents enabling energy-dense and long-

417   cycling lithium metal batteries. Nat. Energy *5*, 526-533.

418 28. Zhang, X.-Q., Chen, X., Hou, L.-P., Li, B.-Q., Cheng, X.-B., Huang, J.-Q., and Zhang, Q. (2019).

419   Regulating anions in the solvation sheath of lithium ions for stable lithium metal batteries. ACS Energy

420   Lett. *4*, 411-416.

421 29. Liu, Y., Lin, D., Li, Y., Chen, G., Pei, A., Nix, O., Li, Y., and Cui, Y. (2018). Solubility-mediated sustained

422   release enabling nitrate additive in carbonate electrolytes for stable lithium metal anode. Nat. Commun. *9*,

423   3656.

424 30. Shi, F., Pei, A., Vailionis, A., Xie, J., Liu, B., Zhao, J., Gong, Y., and Cui, Y. (2017). Strong texturing of

425   lithium metal in batteries. Proc. Natl Acad. Sci. USA *114*, 12138-12143.

426 31. Yan, C., Li, H.-R., Chen, X., Zhang, X.-Q., Cheng, X.-B., Xu, R., Huang, J.-Q., and Zhang, Q. (2019).

427   Regulating the inner helmholtz plane for stable solid electrolyte interphase on lithium metal anodes. J. Am.

428   Chem. Soc. *141*, 9422-9429.

429 32. Wang, T., Zhang, Y., Huang, B., Cai, B., Rao, R.R., Giordano, L., Sun, S.-G., and Shao-Horn, Y. (2021).

430   Enhancing oxygen reduction electrocatalysis by tuning interfacial hydrogen bonds. Nat. Catal. *4*, 753-762.

431 33. Holloczki, O., Macchieraldo, R., Gleede, B., Waldvogel, S.R., and Kirchner, B. (2019). Interfacial domain

432   formation enhances electrochemical synthesis. J. Phys. Chem. Lett. *10*, 1192-1197.

433 34. Huang, C.-J., Thirumalraj, B., Tao, H.-C., Shitaw, K.N., Sutiono, H., Hagos, T.T., Beyene, T.T., Kuo, L.-

434   M., Wang, C.-C., Wu, S.-H., et al. (2021). Decoupling the origins of irreversible coulombic efficiency in

435   anode-free lithium metal batteries. Nat. Commun. *12*, 1452.

436 35. Gauthier, M., Karayaylali, P., Giordano, L., Feng, S., Lux, S.F., Maglia, F., Lamp, P., and Shao-Horn, Y.

437   (2018). Probing surface chemistry changes using $LiCoO_2$-only electrodes in Li-ion batteries. J.

438   Electrochem. Soc. *165*, A1377-A1387.

439   36. Zhang, J.-N., Li, Q., Ouyang, C., Yu, X., Ge, M., Huang, X., Hu, E., Ma, C., Li, S., Xiao, R., et al. (2019).
440   Trace doping of multiple elements enables stable battery cycling of $LiCoO_2$ at 4.6 V. Nat. Energy *4*, 594-
441   603.

442   37. Mao, X.W., Brown, P., Cervinka, C., Hazell, G., Li, H., Ren, Y.Y., Chen, D., Atkin, R., Eastoe, J., Grillo,
443   I., et al. (2019). Self-assembled nanostructures in ionic liquids facilitate charge storage at electrified
444   interfaces. Nat. Mater. *18*, 1350-1357.

445   38. Rakov, D.A., Chen, F.F., Ferdousi, S.A., Li, H., Pathirana, T., Simonov, A.N., Howlett, P.C., Atkin, R., and
446   Forsyth, M. (2020). Engineering high-energy-density sodium battery anodes for improved cycling with
447   superconcentrated ionic-liquid electrolytes. Nat. Mater. *19*, 1096-1101.

448   39. Bi, S., Banda, H., Chen, M., Niu, L., Chen, M., Wu, T., Wang, J., Wang, R., Feng, J., Chen, T., et al. (2020).
449   Molecular understanding of charge storage and charging dynamics in supercapacitors with MOF electrodes
450   and ionic liquid electrolytes. Nat. Mater. *19*, 552-558.

451   40. McOwen, D.W., Seo, D.M., Borodin, O., Vatamanu, J., Boyle, P.D., and Henderson, W.A. (2014).
452   Concentrated electrolytes: decrypting electrolyte properties and reassessing Al corrosion mechanisms.
453   Energy Environ. Sci. *7*, 416-426.

454   41. Wang, F., Borodin, O., Ding, M.S., Gobet, M., Vatamanu, J., Fan, X., Gao, T., Edison, N., Liang, Y., Sun,
455   W., et al. (2018). Hybrid aqueous/non-aqueous electrolyte for safe and high-energy Li-ion batteries. Joule
456   *2*, 927-937.

457   42. Yang, C., Chen, J., Qing, T., Fan, X., Sun, W., von Cresce, A., Ding, M.S., Borodin, O., Vatamanu, J.,
458   Schroeder, M.A., et al. (2017). 4.0 V aqueous Li-ion batteries. Joule *1*, 122-132.

459   43. Suo, L., Borodin, O., Gao, T., Olguin, M., Ho, J., Fan, X., Luo, C., Wang, C., and Xu, K. (2015). "Water-
460   in-salt" electrolyte enables high-voltage aqueous lithium-ion chemistries. Science *350*, 938-943.

461   44. Sun, W., Wang, F., Zhang, B., Zhang, M., Kuepers, V., Ji, X., Theile, C., Bieker, P., Xu, K., Wang, C., and
462   Winter, M. (2021). A rechargeable zinc-air battery based on zinc peroxide chemistry. Science *371*, 46-51.

463   45. Wang, X., Salari, M., Jiang, D.-e., Chapman Varela, J., Anasori, B., Wesolowski, D.J., Dai, S., Grinstaff,
464   M.W., and Gogotsi, Y. (2020). Electrode material-ionic liquid coupling for electrochemical energy storage.
465   Nat. Rev. Mater. *5*, 787-808.

466   46. Bayaguud, A., Luo, X., Fu, Y., and Zhu, C. (2020). Cationic surfactant-type electrolyte additive enables
467   three-dimensional dendrite-free zinc anode for stable zinc-ion batteries. ACS Energy Lett. *5*, 3012-3020.

468   47. Dubouis, N., Serva, A., Berthin, R., Jeanmairet, G., Porcheron, B., Salager, E., Salanne, M., and Grimaud,
469   A. (2020). Tuning water reduction through controlled nanoconfinement within an organic liquid matrix.
470   Nat. Catal. *3*, 656-663.

471   48. Wagner, A., Sahm, C.D., and Reisner, E. (2020). Towards molecular understanding of local chemical
472   environment effects in electro- and photocatalytic CO_2 reduction. Nat. Catal. *3*, 775-786.

473   49. You, Y., Yu, X., Yin, Y., Nam, K.-W., and Guo, Y.-G. (2015). Sodium iron hexacyanoferrate with high Na
474   content as a Na-rich cathode material for Na-ion batteries. Nano Res. *8*, 117-128.

475   50. Van Der Spoel, D., Lindahl, E., Hess, B., Groenhof, G., Mark, A.E., and Berendsen, H.J.C. (2005).
476   GROMACS: Fast, flexible, and free. J Comput Chem *26*, 1701-1718.

477   51. Park, C., Kanduc, M., Chudoba, R., Ronneburg, A., Risse, S., Ballauff, M., and Dzubiella, J. (2018).
478   Molecular simulations of electrolyte structure and dynamics in lithium-sulfur battery solvents. J. Power
479   Sources *373*, 70-78.

480   52. Rappé, A.K., Casewit, C., Colwell, K.S., Goddard, W.A., and Skiff, W.M. (1992). UFF, a full periodic table

481   force field for molecular mechanics and molecular dynamics simulations. J. Am. Chem. Soc. *114*, 10024-
482   10035.

483 53. Ebadi, M., Costa, L.T., Araujo, C.M., and Brandell, D. (2017). modelling the polymer electrolyte/li-metal
484   interface by molecular dynamics simulations. Electrochim. Acta *234*, 43-51.
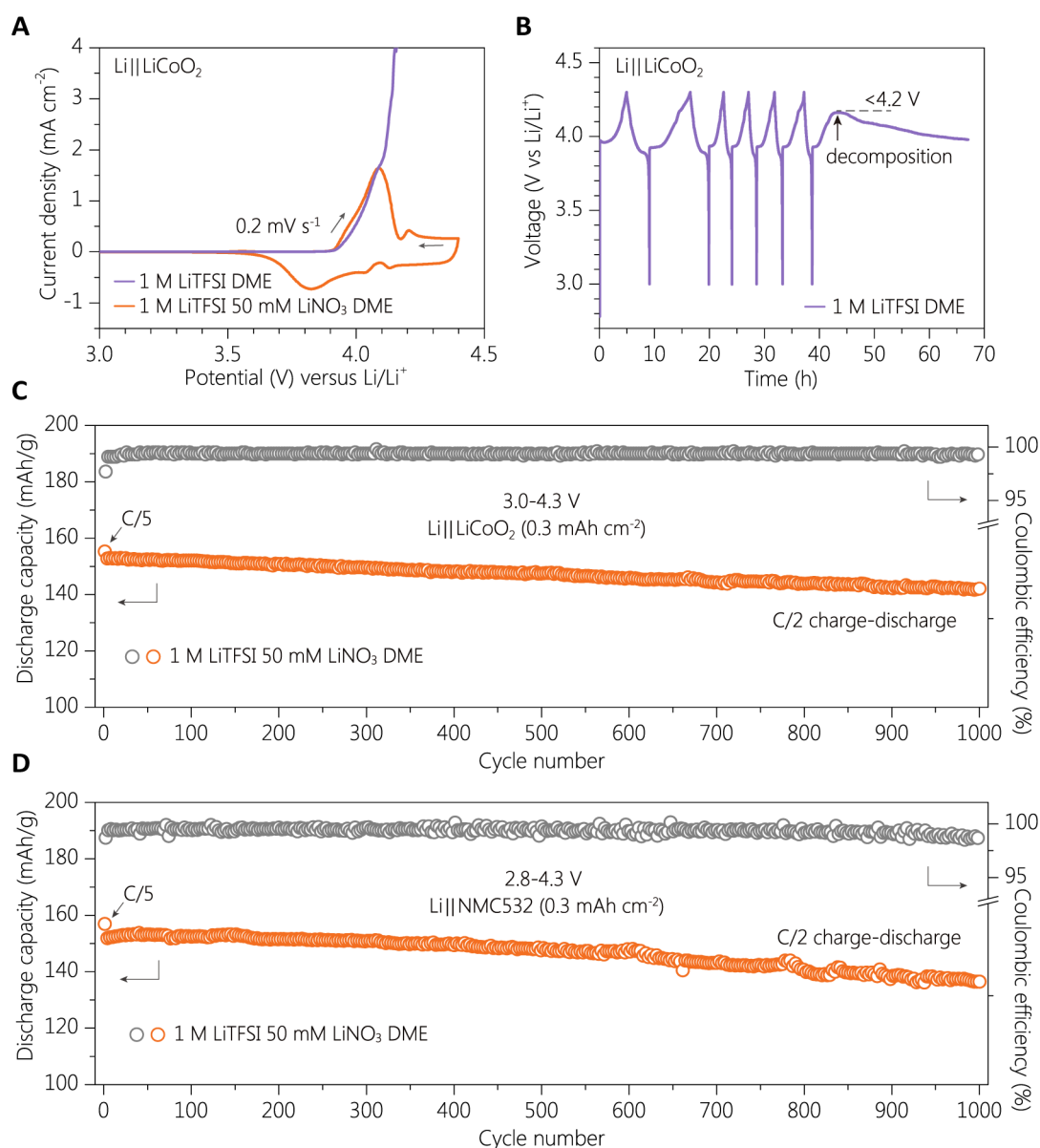
Figure 1. Electrochemical behavior of ether electrolytes in Li∥LiCoO₂ and Li∥NMC532 batteries.
(A) CV curves of the NO_3^--containing and NO_3^--free dilute ether electrolytes with $LiCoO_2$ cathodes as working electrodes in Li∥LiCoO₂ coin cells. (B) Voltage profile of Li∥LiCoO₂ coin cell with 1 M LiTFSI DME. (C and D) Cycling performance of (C) Li∥LiCoO₂ and (D) Li∥NMC532 batteries in the NO_3^--containing dilute ether electrolyte under 4.3 V charge cutoff voltage.
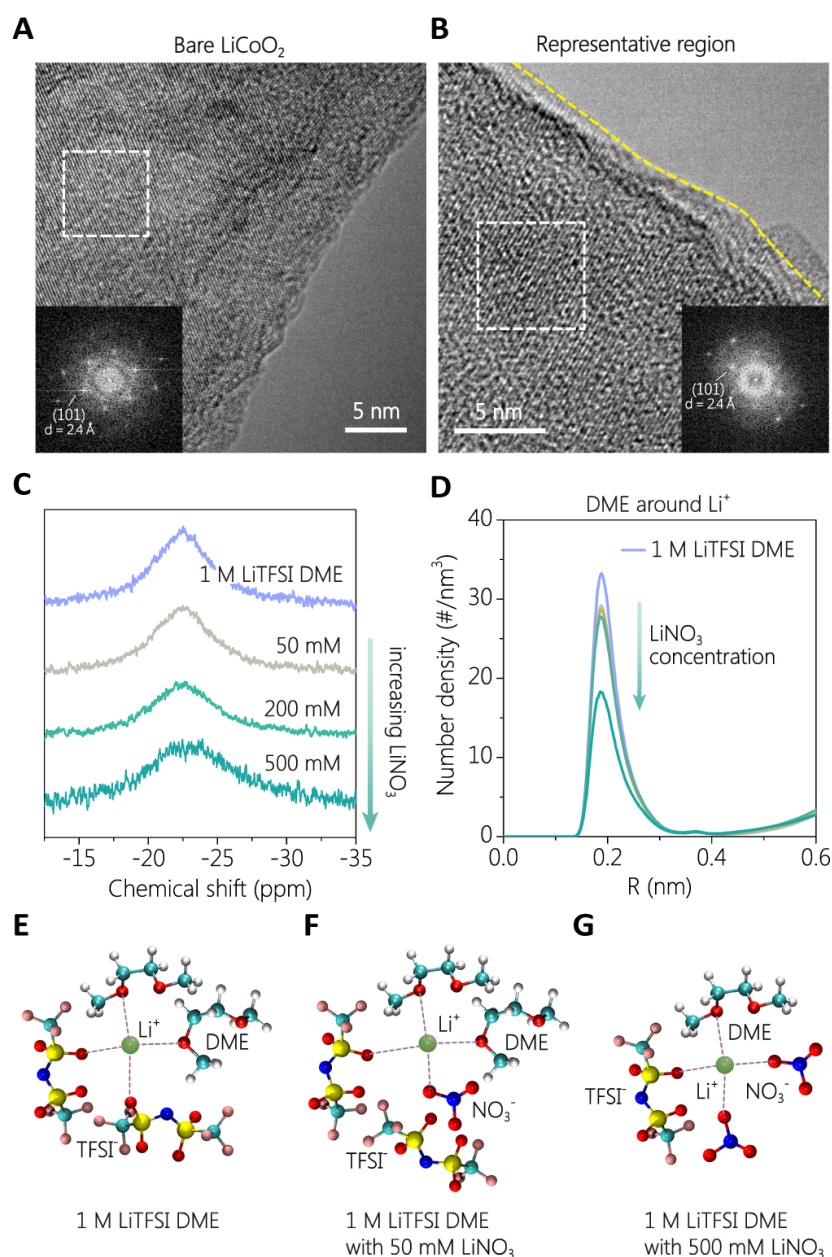
Figure 2. Analysis of the electrolyte decomposition and solvation structure in the presence of nitrate.

(A and B) TEM images of (A) bare $LiCoO_2$, (B) representative region of cycled $LiCoO_2$ electrode (50 cycles) under charge cutoff voltage of 4.3 V in 1 M LiTFSI 50 mM $LiNO_3$ DME electrolyte. Insets are the fast Fourier transform (FFT) patterns of selected regions.
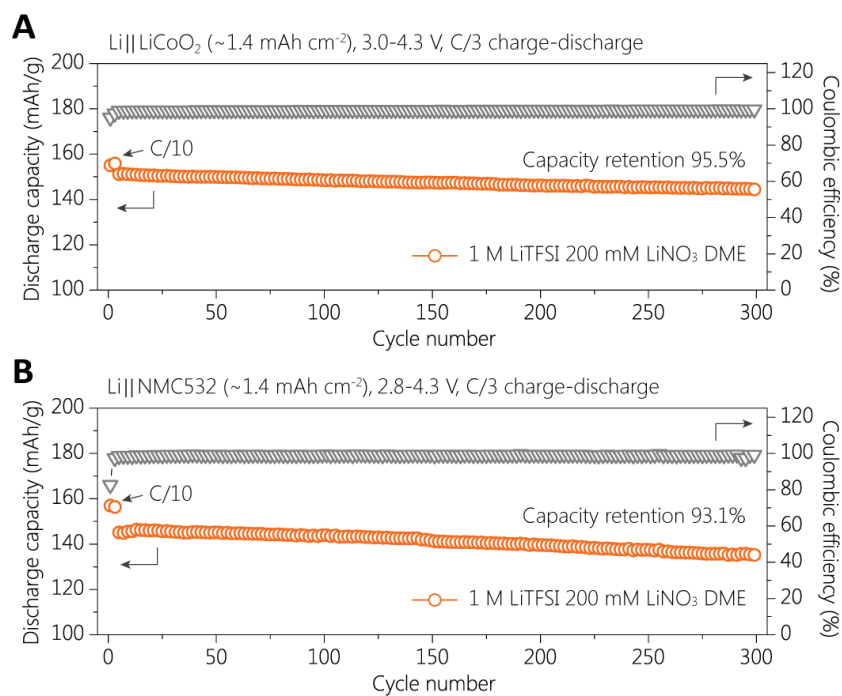
(C and D) (C) ^{17}O-NMR and (D) radial number density of DME around Li^+ of 1 M LiTFSI DME electrolyte (top blue) and 1 M LiTFSI DME with increasing $LiNO_3$ concentration (bottom green).

(E–G) Solvation structure of (E) 1 M LiTFSI DME, (F) 1 M LiTFSI DME with 50 mM $LiNO_3$, and (G) 1 M LiTFSI DME with 500 mM $LiNO_3$ given by MD simulations. Colour scheme in E–G: green, Li; pink, F; red, O; light blue, C; navy, N; yellow, S; silver gray, H.
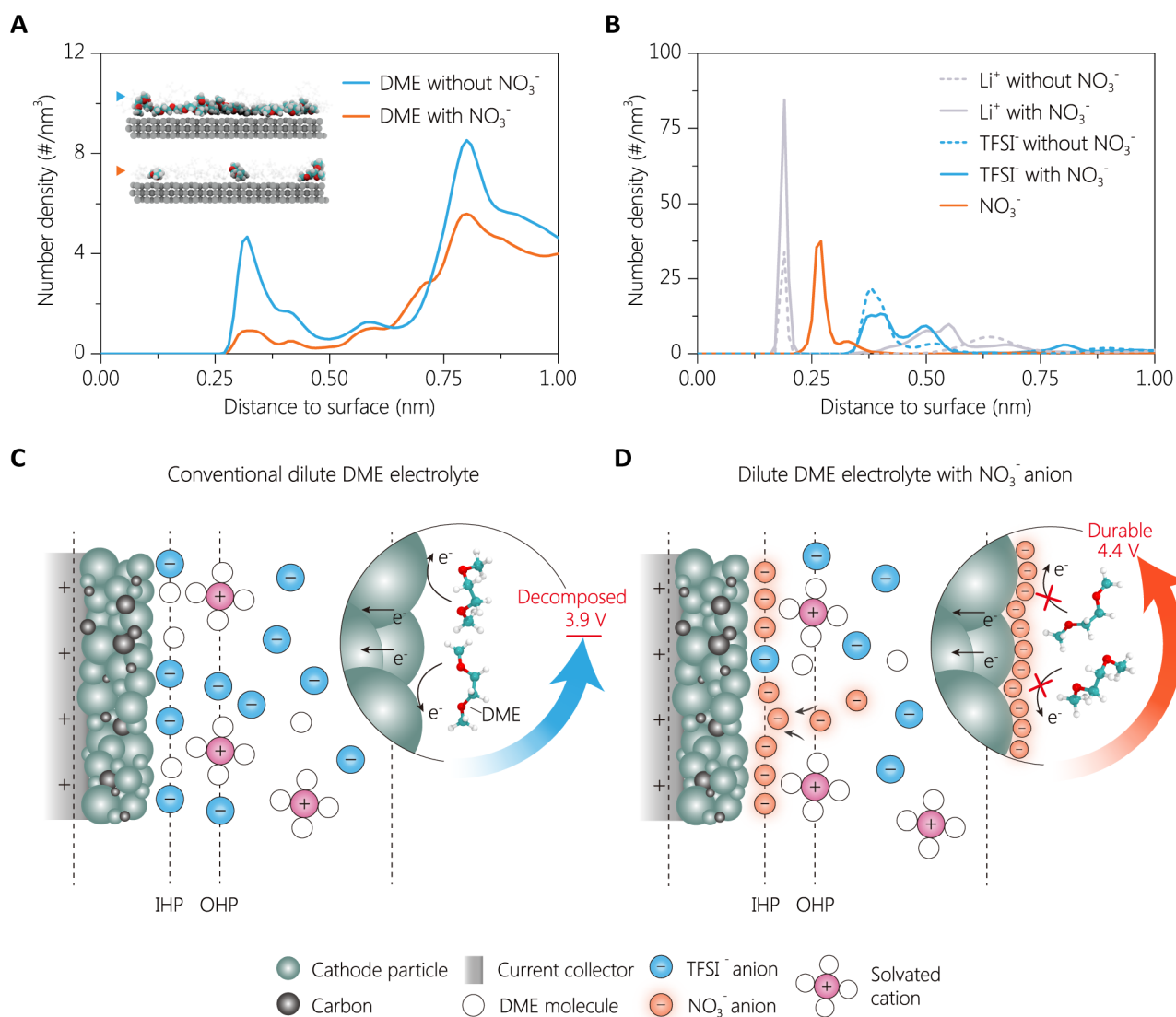
**Figure 3. Ion and DME distributions at electrified LiCoO$_2$ interfaces and their effect on DME decomposition.**

(A and B) The number density along with the distance from the surface of LiCoO$_2$ of (A) DME and (B) ions at 1.2 V in NO$_3^-$-free/containing electrolytes. (C) Schematics of interfacial adsorption and charge transfer process on the positive electrode in a conventional dilute electrolyte. (D) Proposed mechanism for the solvent-exclusion in the presence of NO$_3^-$. NO$_3^-$ adsorption prevents DME molecules from being adsorbed, thus preventing the breakdown of DME. IHP, inner Helmholtz plane. OHP, outer Helmholtz plane. For clarity, the Li$^+$ ion distributions near the electrode surface are not shown in schematic diagrams.

21

A Li‖LiCoO$_2$ (~1.4 mAh cm^{-2}), 3.0-4.3 V, C/3 charge-discharge

C/10

Capacity retention 95.5%

1 M LiTFSI 200 mM LiNO$_3$ DME

B Li‖NMC532 (~1.4 mAh cm^{-2}), 2.8-4.3 V, C/3 charge-discharge

C/10

Capacity retention 93.1%

1 M LiTFSI 200 mM LiNO$_3$ DME

512

Figure 4. Electrochemical performances of Li‖LiCoO$_2$ and Li‖NMC532 cells in ether electrolytes under higher areal capacities.

(A and B) Cycling stability of (A) Li‖LiCoO$_2$ and (B) Li‖NMC532 batteries in 1 M ether electrolyte with 200 mM LiNO$_3$ under 4.3 V charge cutoff voltage. The Li‖cathode cells were charged and discharged at a C/3 rate after formation cycles at C/10, where 1C equals to 1.37 mA cm^{-2} for LiCoO$_2$ cathode and 1.56 mA cm^{-2} for NMC532 cathode, respectively.
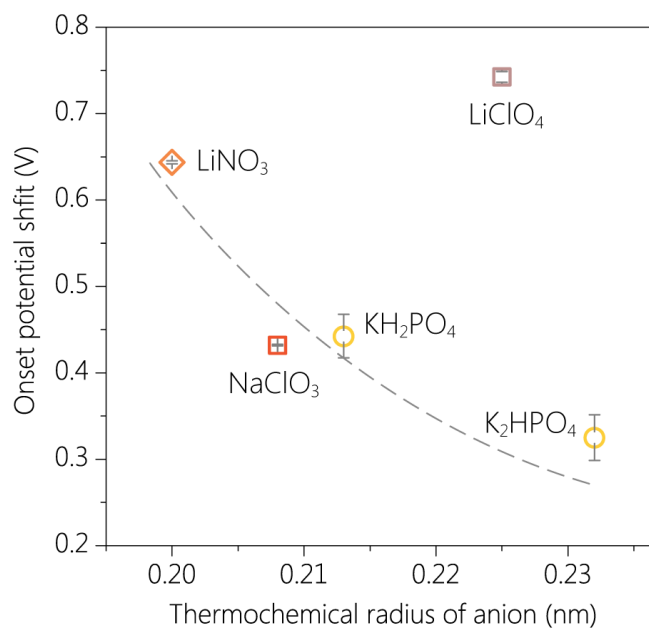
Figure 5. Impact of the additive anion type on the oxidation stability of ethers.
Relationship between onset potential shift and corresponding thermochemical radius of the anion. The error bars are collected from the linear sweep voltammetry tests of electrolytes with different salt additives (Table S1). The nearly linear shape for the onset potential shift with additive anion radius suggests that the geometric size of anion matters to the ion interfacial packing. The dashed line is a guide for the eyes.